Size Distributions of Gold Nanoclusters Studied by Liquid Chromatography

J. P. Wilcoxon,* J. E. Martin, and P. Provencio

Nanostructures and Advanced Materials, Chemistry Department, Department 1122, Sandia National Labs, Albuquerque, New Mexico 87185

Received May 15, 2000. In Final Form: August 29, 2000

We report high-pressure liquid chromatography (HPLC) and transmission electron microscopy (TEM) studies of the size distributions of nanosize gold clusters dispersed in organic solvents. These metal clusters are synthesized in inverse micelles at room temperature, and those investigated range in diameter from 1 to 10 nm. HPLC is sensitive enough to discern changes in hydrodynamic volume corresponding to only 2 carbon atoms of the passivating agent or metal core size changes of less than 4 Å. We have determined for the first time how the total cluster volume (metal core + passivating organic shell) changes with the size of the passivating agent.

I. Introduction

Over a century ago, the realization that certain closed shell electron arrangements lead to special chemical stability in atoms led to the development of the periodic table and a simple understanding of bonding in molecules.[1] More recently, nuclear chemists have argued that certain "magic" numbers of protons and neutrons convey extraordinary stability to certain nuclei as well and have developed a shell model of the nucleus analogous to that of atomic electronic shells.[2] Of direct relevance to the present work is the observation that clusters of certain "free-electron" metallic atoms such as Na, formed in atomic beam experiments and studied by mass spectrometry, MS, show certain especially abundant peaks in their mass size distribution that correspond to closed shells of valence electrons (the ionic Na nuclei forming the core of a giant "molecule").[3,4] An open question is whether these "magic" sizes will predominate in liquid-based synthesis, using surfactants to restrict the growth. It is likely that these magic sizes will be important if cluster stability plays an important role in the nanocluster growth mechanism.

To study the importance of magic sizes for solution grown nanoclusters, new size characterization tools are needed to supplement traditional approaches such as mass spectrometry (MS) or high resolution transmission electron microscopy (HRTEM). For clusters formed in the gas phase, MS is a useful and easy-to-apply size analysis tool to determine mass distributions that has allowed scientists to investigate clusters of free-electron metals formed by gas-phase aggregation.[5] However, for clusters formed in the liquid phase by chemical approaches, a means of aerosolizing and ionizing inorganic nanoclusters and interfacing the high-pressure liquid environment to the high-vacuum gas environment of the MS must be found. This is a complex and challenging problem, and only one group has been able to apply MS analysis successfully to clusters formed by liquid-phase synthesis.[6] Alvarez and co-workers used laser desorption of the nanoclusters from a solid matrix to form the aerosol. However, as these authors correctly noted, the issue of cluster mass fragmentation during ionization and laser desorption, combined with the relatively poor sensitivity of typical time-of-flight MS detectors to high MW ions, makes this approach difficult. There is also the very real difficulty of obtaining calibration standards of a similar chemical nature, narrow size distribution, and predictable ionization pattern.

It seems reasonable that, just as clusters synthesized in the gas phase are most easily studied by gas-phase detectors, clusters synthesized in liquid phases should be studied by liquid-phase approaches and detectors that can respond to clusters in liquids. One possibility is the use of dynamic light scattering (DLS) to determine the rate of cluster diffusion in a liquid, and thus the average cluster radius. However, in the case of strongly light absorbing, weakly scattering (i.e., nanosize) inorganic nanoclusters like gold or silver, this approach is impractical because of low signal-to-noise, (S/N). Even in the case of larger, strongly scattering clusters that have some size dispersion, DLS cannot separate out the contribution of each size cluster in the population to the total correlation function, and thus, a separate fractionation method is still required for a satisfactory analysis.

Similarly, other small-angle static scattering techniques using neutrons or X-rays (e.g., SAXS) to obtain size dispersion information rely on a specific model (e.g., noninteracting polydisperse spheres with a Gaussian or other assumed distribution of sizes) to extract information from the depth and number of oscillations in the form factor, $S(qR)$.[7] However, most of these oscillations will actually occur in an inaccessible q regime $qR \gg 1$ for very small clusters (e.g., R ∼ 5 nm means $q \gg 0.2$ nm^{-1}), where q is the momentum transfer and R the sphere radius, and thus, at best, only one or two oscillations in $S(qR)$ will be experimentally observed, except when using an intense X-ray source (e.g., a synchrotron) and an efficient Bonse-Hart detector. Even in this case, data must be collected

* To whom correspondence should be addressed.

(1) Pauling, L. *The Nature of the Chemical Bond and the Structure of Molecules and Crystals; An Introduction to Modern Structural Chemistry*, 3rd ed.; Cornell University Press: Ithaca, NY, 1960.

(2) Friedlander, G.; Kennedy, J. W.; Miller, J. M. *Nuclear and Radiochemistry*, 2nd ed.; John Wiley & Sons: New York, 1966.

(3) de Heer, W. A. *Rev. Mod. Phys.* **1993**, *65*, 612.

(4) Brack, M. *Rev. Mod. Phys.* **1993**, *65*, 677.

(5) Yamada, Y.; Castleman, A. W., Jr. *J. Chem. Phys.* **1992**, *97*, 4543.

(6) Alvarez, M. M.; Vezmar, I.; Whetten, R. L. *J. Aerosol Sci.* **1998**, *29*, 115.

(7) Wilcoxon, J. P.; Craft, S. A.; Thuston, T. R. *Rev. Sci. Instrum.* **1996**, *67*, 3021.

10.1021/la000669j CCC: $19.00
Published on Web 10/31/2000

Table 1. Recipes for Au Nanocluster Synthesis Using Inverse Micelles

sample #	[Au][a]	surfactant	solvent	reductant	post-synthesis passivator[b]
463, a	$NaAuCl_4$	C12E5(10 wt %)	C8	SuperH(0.04M)/thf	none, C12SH
469, a, b, c	$HAuCl_4$	C12E5(10 wt %)	C8	LSelAlH(0.04M)/thf	none, C8SH, C12SH, C16SH
470, a, b, c	$HAuCl_4$	C12E5(10 wt %)	C8	$LiAlH_4$(0.04M)/tol	none, C8SH, C12SH, C16SH
486, a, b, c	$(NH_4)AuCl_4$	C12E6(10 wt %)	C10	$LiAlH_4$(0.04M)/tol	none, C6SH, C10SH, C18SH
487, b, c, d	$(NH_4)AuCl_4$	C12E6(10 wt %)	C10	$LiAlH_4$(0.04M)/tol	none, C12SH, C12SH,[c] C12SH[d]
492, a, b, c	$HAuCl_4$	C12E5(10 wt %)	C16	$LiAlH_4$(0.08M)/tol	none, C6SH, C10SH, C14SH
508, p	$HAuCl_4$	TOAB(0.06M)/C12SH(0.01M)	toluene	$NaBH_4$(0.1M)/H_2O	none, purified
511, bp	$HAuCl_4$	TOAB(0.06M)	toluene	$NaBH_4$(0.1M)/H_2O	none, C12SH/purified
514c, cp	$HAuCl_4$	DDAB(0.094M)	toluene	$LiAlH_4$(0.04M)/thf	C12SH, purified
516c, cp	$HAuCl_4$	TOAB(0.06M)	toluene	$LiAlH_4$(0.04M)/thf	C12SH, purified
519a	$HAuCl_4$	THAC(10 wt %)	toluene	$LiAlH_4$(0.04M)/thf	C12SH
521c, cp	$HAuCl_4$	AOT(10 wt %)	toluene	$LiAlH_4$(0.04M)/thf	C12SH, purified
536	$HAuCl_4$	TOAB(0.06M)/C12SH(0.005M)	toluene	$NaBH_4$(0.1M)/H_2O	none
537	$HAuCl_4$	TOAB(0.06M)/C12SH(0.02M)	toluene	$NaBH_4$(0.1M)/H_2O	none
538	$HAuCl_4$	TOAB(0.06M)/C12SH(0.03M)	toluene	$NaBH_4$(0.1M)/H_2O	none
539	$HAuCl_4$	TOAB(0.06M)	toluene	$NaBH_4$(0.1M)/H_2O	none
565, ap, bp, cp	$HAuCl_4$	TOAB(0.06M)	toluene	$NaBH_4$(0.1M)/H_2O	none, C8SH,[e] C12SH,[e] C16SH[e]
565p	$HAuCl_4$	TOAB(0.06M)/C8SH(0.03M)	toluene	$NaBH_4$(0.1M)/H_2O	none
566p	$HAuCl_4$	TOAB(0.06M)/C12SH(0.03M)	toluene	$NaBH_4$(0.1M)/H_2O	none
567p	$HAuCl_4$	TOAB(0.06M)/C16SH(0.03M)	toluene	$NaBH_4$(0.1M)/H_2O	none

[a] All [Au] = 0.01 M unless otherwise noted. [b] Thiol Added @ 0.01 M @ 1 h after reduction unless otherwise noted. [c] C12SH @ 14 days. [d] C12SH @ 26 days. [e] CkSH @ 0.03 M, purified. Abbreviations: SuperH = $Li(C_2H_5)_3H$, LSelAlH = $LiAl(OC(CH_3)_3)_3H$, DDAB = didodecyldimethylammonium bromide, TOAB = tetraoctylammonium bromide, THAC = tetrahexylammonium chloride, AOT = Aerosol-OT.

over several hours, and the information obtained is still only sufficient to obtain an average size, not the size dispersion.

Thus, scientists who wish to characterize the size distribution of solution-grown nanoclusters have relied almost exclusively on TEM and HRTEM. Unfortunately, inferring ensemble average properties such as average diameter or shape based on the limited regions examined in typical TEMs is akin to determining the street layout of New York city by examining a square centimeter of side walk—it just is not statistically significant. This statistical uncertainty occurs partly due to human subjectivity when deciding which areas of the grid to image and photograph but also is due to size segregation effects during the drying process, which may give rise to a nonrepresentative sample of clusters in a given region. Additionally, for clusters smaller than about 2−3 nm, just determining the boundary between a cluster and grid is challenging, and the size uncertainty in HRTEM is at least one lattice plane or about 10% of the average size. So, even if an ensemble of nanoclusters in the nanosize range were perfectly monodisperse, measurement uncertainly alone would cause one to infer a 5−10% spread in cluster size. It is interesting to note that such size dispersion is just what most researchers commonly quote for their TEM measurements. An additional difficulty, often ignored, lies in the process of drying clusters out on a grid. This process can cause size changes to the clusters, induce aggregation, or lead to chemical changes (e.g., oxidation) of the clusters. And, of course, one can neither see the organic groups used to passivate a cluster surface using electrons nor determine the size of this organic "shell".

Though we are by no means advocating the abandonment of TEM approaches to *qualitative* cluster analysis, we hope to demonstrate that liquid chromatography, an approach traditionally used to separate molecules and polymers by size, shape, and chemical properties, can be used to analyze cluster size distributions and the effects of aging and passivating molecules while simultaneously obtaining the optical properties (e.g., absorbance and fluorescence) and other physical properties (e.g., conductivity) of the clusters. Such studies can be done on a single sample using a volume of only 10 μL, with an analysis time of 15−20 min and a size resolution of better than 2 Å, which represents the true, unbiased ensemble average of the size and optical properties of the solution. Such studies are the subject of this paper.

II. Experimental Section

Nanocluster Synthesis. We have described our approach to nanocluster synthesis using inverse micelles extensively in a series of papers.[8−11] Here, we add some details relevant to this work. Our approach has changed only in minor ways since our first description of metal nanocluster synthesis in 1989.[8] The most significant change is the use of strongly binding surfactants,[12] thiols, to passivate the surface during or after the chemical reduction, which allowed us to employ HPLC analysis of the nanocluster size and size dispersion. When thiols are added prereduction, they can significantly alter the final nanocluster size, since they inhibit the cluster growth more strongly than the nonionic and cationic surfactants we typically use to solubilize the gold salts in inverse micelles. However, the use of alkanethiols as passivating agents presents other issues that we will discuss in a later paper, namely, certain alkanethiols act as etchants, reducing the size of the as-synthesized clusters. They also fail to bind as effectively to larger (e.g., $d > 4$ nm) Au clusters as they do to smaller ones (e.g., $d < 2-3$ nm). The thiols, though present in much lesser amounts than the surfactants used to form the inverse micelles, compete very effectively for binding sites on the growing nanocluster surface. Due to their strong binding properties, thiol passivating agents also permit purification and removal of ionic byproducts and most of the surfactant micelles used to solubilize the metal salt precursors. The stabilization of the nanocluster surface by a strongly binding ligand is critical to the variety of purification approaches described in the Results section.

Since we have previously described our general inverse micelle approach to nanocluster synthesis,[9,10] we will not repeat the details here but will refer the reader to Table 1 of this paper. Subsequently, numerous other papers describing Au nanocluster synthesis using so-called phase transfer catalysts (i.e., cationic

(8) Wilcoxon, J. P.; Williamson, R. L. *Proceedings of the Fall Meeting of the MRS*, 1989.
(9) Wilcoxon, J. P. U.S. Patent 5,147,841, September 15, 1992.
(10) Wilcoxon, J. P.; Williamson, R. L.; Baughman, R. J. *J. Chem. Phys.* **1993**, *98*, 9933.
(11) Wilcoxon, J. P.; Samara, G. A. *Phys. Rev. B* **1995**, *51*, 7299.
(12) Whetten, R. L.; Khoury, J. T.; Alvarez, M. M.; Murthy, S.; Vezmar, I.; Wang, Z. L.; Stephens, P. W.; Clevelend, C. L.; Luedtke, W. D.; Landman, U. *Adv. Mater.* **1996**, *8*, 428.

Table 2. HPLC Size Properties of Synthesized Au Nanoclusters

sample #	column	t_r(min) ± Δt_r	D_h(nm)	D_{core}(nm)[a]	D_{core}(nm)[b]	k, shell(nm)
463	pl500	6.05 ± 1.0	7.38	5.1	5.0 ± 1	12, 2.28
469a	pl500	6.81 ± 0.44	4.82	3.08 ± 0.4		8, 1.74
469b	pl500	6.61 ± 0.42	5.39	2.9 ± 0.4	2.8 ± 0.3	12, 2.46
469c	pl500	6.44 ± 0.48	5.93	2.73 ± 0.5		16, 3.2
470a	pl500	6.99 ± 0.41	4.36	2.62 ± 0.3		8, 1.74
470b	pl500	6.77 ± 0.37	4.93	2.45 ± 0.2	2.0 ± 0.4	12, 2.46
470c	pl500	6.60 ± 0.39	5.43	2.23 ± 0.3		16, 3.2
486a	pl500	7.46 ± 0.54	3.35	1.93 ± 0.4		6, 1.42
486b	pl500	7.10 ± 0.6	4.10	2.00 ± 0.6		10, 2.10
486c	pl500	6.65 ± 0.47	5.28	1.98 ± 0.5		18, 3.30
487b	pl1000	8.0 + 0.45	4.17	1.80 ± 0.2	2.0 ± 0.2	12, 2.46
487d	pl1000	6.73 ± 0.55	9.0	6.5 ± 0.6	6.2 ± 0.5	12, 2.46
492a	pl1000	8.300 ± 0.4	3.39	2.0 ± 0.2	2.0 ± 0.2	6, 1.39
492a	pl500	7.42 ± 0.54	3.42	2.0		6, 1.42
492a	HR3	9.02 ± 0.5	3.36	2.0		6, 1.36
492a	pl1000 × 2	15.43 ± 0.6	3.13	1.74		6, 1.39
492b	pl1000	7.96 ± 0.4	4.19	2.0 ± 0.2	2.0 ± 0.2	10, 2.19
492b	pl500	7.10 ± 0.45	4.10	2.0		10, 2.10
492b	HR3	7.96 ± 0.5	4.07	2.0		10, 2.07
492b	pl1000 × 2	14.75 ± 0.6	3.89	1.70		10, 2.19
492c	pl1000	8.23 ± 0.4	4.87	2.0 ± 0.2	2.0 ± 0.2	14, 2.87
492c	pl500	6.87 ± 0.44	4.66	2.0		14, 2.66
492c	HR3	7.96 ± 0.5	4.70	2.0		14, 2.70
492c	pl1000 × 2	14.16 ± 0.7	4.70	1.83		14, 2.87
508p	pl1000	7.86 ± 0.4	4.46	2.0 ± 0.2	2.0 ± 0.2	12, 2.46
508p	pl500	6.93 ± 0.42	4.51	2.03		12, 2.46
508p	pl1000 × 2	14.27 ± 0.6	4.54	2.08		12, 2.46
511bp	pl1000	7.24 ± 0.5	6.57	4.1 ± 0.5	3.8 ± 0.5	12, 2.46
514cp	pl1000	8.15 ± 0.4	3.72	1.26 ± 0.2		12, 2.46
516cp	pl1000	8.0 ± 0.4	4.09	1.63 ± 0.2		12, 2.46
519a	pl1000	7.26 ± 0.4	6.49	4.03 ± 0.2	4.2 ± 0.4	12, 2.46
521cp	pl1000	7.81 ± 0.4	4.60	2.14 ± 0.2		12, 2.46
536	pl1000	7.90 ± 0.35	4.35	1.90 ± 0.06	2.0 ± 0.2	12, 2.46
537	pl1000	7.97 ± 0.35	4.17	1.70 ± 0.06	1.8 ± 0.2	12, 2.46
538	pl1000	8.05 ± 0.35	3.96	1.60 ± 0.06	1.8 ± 0.2	12, 2.46
539	HR3	6.3 ± 1.0	10.7	8.24		12, 2.46
564ap	pl1000	7.72 ± 0.6	4.87	3.2 ± 0.7		8, 1.67
564bp	pl1000	7.52 ± 0.45	5.51	2.8 ± 0.3	3.0 ± 0.6	12, 2.46
564cp	pl1000	7.38 ± 0.5	6.02	3.06 ± 0.5	3.1 ± 0.8	16, 3.22
565p	pl1000	8.30 ± 0.3	3.39	1.72 ± 0.0	1.8 ± 0.3	8, 1.67
566p	pl1000	7.98 ± 0.3	4.14	1.68 ± 0.0	1.6 ± 0.3	12, 2.46
567p	pl1000	7.80 ± 0.3	4.63	1.41 ± 0.0	1.7 ± 0.3	16, 3.22

[a] From HPLC. [b] from TEM or HRTEM.

surfactants)[12,13] have been published. There are some misconceptions about the role of the cationic surfactants used in these synthetic approaches. The first is that the typical recipe requires water to first dissolve the salt (typically $HAuCl_4$ or $NaAuCl_4$) and then requires this aqueous salt solution to be brought into contact with an immiscible toluene solution containing a cationic surfactant (usually tetraoctylammonium bromide (TOAB)). The first issue is why only certain cationic surfactants will actually solubilize the gold salt into the organic phase. The reason is that very hydrophobic (i.e., long-chain alkyl) surfactants are required to ensure both the formation of spherical micelles in the organic (toluene) phase and the total exclusion of water from that phase. Because such cationic surfactants spontaneously form inverse micelles in toluene, as discovered several years ago by neutron scattering,[8] they are capable of directly solubilizing a wide variety of metal salts without the use of water. We have described such an inverse micelle synthesis in ref 10 and in our patent, ref 9, using didodecyldimethylammonium bromide (DDAB) in toluene. All other recipes in the literature use TOAB to solubilize the metal salt, but as we demonstrate, (see Table 2), the particular cationic surfactant used has a minor effect on the final nanocluster size, provided the [Au]:[surfactant] ratio is identical, the counterion is invariant, and the reducing agent is not changed.

With this general understanding of the role of the cationic surfactant as a micelle-forming agent that can directly solubilize a variety of metal salts, water need not be introduced into the system, thus allowing the use of strong reducing agents such as $LiBH_4$ in tetrahydrofuran (THF) or $LiAlH_4$ in THF or toluene. These reducing agents are generally superior to $NaBH_4$ in water, which is typically used to reduce $HAuCl_4$ in two-phase systems. Even if one chooses to use $NaBH_4$ as a reductant, because $NaBH_4$ in neutral aqueous solution is unstable with respect to hydrolysis, only highly alkaline solutions (~4 NaOH:$NaBH_4$) should be used to effect reductions. Such caustic reducing solutions are quite stable; they are actually sold by Aldrich as stock (~4.4 M $NaBH_4$ in ~14 M NaOH solutions) and can be diluted into water, as desired.

In the case of gold or silver, the precursor metal salts are so easily reduced that the use of alkaline $NaBH_4$ in water, as we described in our earlier work, is quite acceptable. However, this reducing agent is somewhat ineffective for the reduction of Pt or Pd salts and is completely ineffective for formation of metallic Fe, Ni, Co, Si, or Ge. Instead, in the case of Fe, Ni, or Co, the corresponding metal boride will form.

High-Pressure Liquid Chromatography. HPLC approaches to separation are of two basic types. The first relies on the different chemical affinities of molecules for different surface chemical groups attached to solid media, typically porous SiO_2. This approach depends on the different affinities for molecules in the solid or stationary phase of the column as compared to the mobile phase (the liquid), which transports the molecules under high pressure (typically 800−2000 psi) to separate the molecules in time. This mechanism is relatively insensitive to the size differences between molecules but very sensitive to their chemical functionalities; for example, toluene can be easily separated from phenol. The second approach, the subject of this paper, uses porous hydrophobic microgels (typically cross-linked polystyrene)

(13) Brust, M.; Fink, J.; Bethell, D.; Schriffin, D. J.; Kiely, C. *J. Chem. Soc., Chem. Commun.* **1995**, 1655.

to separate molecules by size. It is commonly called size exclusion chromatography (SEC).[14] The basic principal of SEC is simple—large molecules cannot penetrate the pores of the column media as effectively as small ones; as a result, they spend less time exploring the pore structure of the column and elute through the column faster than small ones. The size range of applicability of a typical SEC column varies with the average pore size of the column, which ranges from 50 Å to >100 000 Å in commercially available columns (Polymer Labs (PL series), Waters Corp. (HR series)) A 50-Å column will easily separate hydrocarbons differing in size by 2 carbons (e.g., hexane from octane), whereas a 100 000-Å column will separate large polymers with molecular weights of more than 1 000 000 Da.

The key to the application of SEC to the analysis of inorganic nanoclusters is effective surface passivation of the clusters using nonpolar organic ligands. This is because SEC columns were designed to have little or no specific chemical affinity for nonpolar organic molecules but have a great tendency to permanently adsorb bare inorganic ions or inorganic clusters. These columns must also be used with fairly nonpolar mobile phases such as toluene or tetrahydrofuran (THF). This is perhaps the explanation for their very limited application in inorganic colloidal materials,[15,16] most of which are traditionally synthesized in water. Our goal is to trick the column into believing that a passivated inorganic cluster is just a large, nonsticky organic entity like polystyrene, so that it will simply meander through the pores, gradually getting separated from any other clusters and/or molecules with either a different size or shape.

The variety of detectors suitable for use with HPLC separation is large and even includes mass spectrometers (not yet suitable for the molecular weights nor ionization requirements of inorganic nanoclusters). We find that the most useful and versatile detectors for metal nanoclusters are the photodiode array (PDA)-based UV−visible absorbance detector and refractive index (RI) types. The former collects the entire absorbance spectrum from 200 to 800 nm at a rate of about 1−2 spectra/second and has a user-selectable bandwidth of 1.2−4.8 nm. The wavelength range of the data collected is limited by the mobile phase transparency, which only extends to about 290 nm, for example, for toluene. Since the elution peak widths are at least 20 s, spectral information is available even within the eluting peak. In addition, the sensitivity of these detectors is remarkable, noise levels being 10^{-5} AU for the PDA, for example.

An RI detector is useful for detecting non- or weakly light-absorbing species, such as surfactants or other chemical impurities, and byproducts of the reaction and to verify that nanocluster purification schemes are effective. The RI detector works by measuring the differential refraction between the mobile phase, held in a reference cell, and the analyte when it passes through the detector cell. We use a conductivity detector instead of the RI detector for high sensitivity to conducting species such as salts or cationic surfactants. In this case, a conducting mobile phase-like THF must be used. Signals are routinely obtained from 10^{-8} M of 10 μL of a metal salt. These detectors allow the determination of the optical absorbance and size distribution of a nanocluster sample in about 15 min using 10 μL of sample at a Au concentration of only 0.001 M to 0.01M!

III. Results and Discussion

In Table 1, we show recipes for the synthesis of selected samples whose HPLC characterization is described in this paper in Table 2. In this table, our sample names consist of a number, which denotes the sequential synthesis number of the sample, a letter, which indicates that some type of organic passivating agent was added postsynthesis, and a "p" that is appended to the sample number and/or letter, denoting whether it was chemically purified from its reaction byproducts and excess surfactants by one of the approaches described below. In this table, we use the common abbreviation C*i*E*j* for nonionic surfactants consisting of *i* CH_2−units of an alkyl hydrophobic tail group attached to *j* CH_2CH_2O−units of a hydrophilic ether headgroup. These alkylated polyethers commonly are obtained in ultrapure form from Nikko Chemicals, Japan. Other abbreviations for the reducing agents and cationic surfactants are given in the footnotes to Table 1.

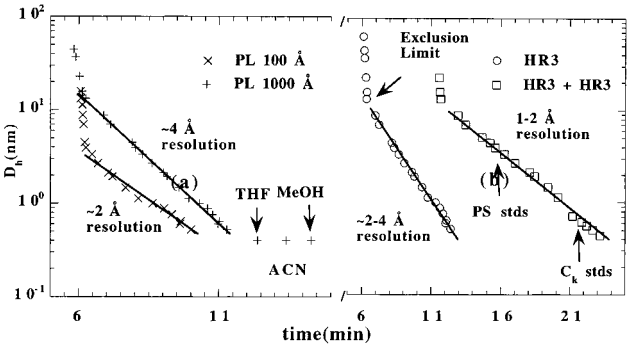

Figure 1. Hydrodynamic diameter (D_h) vs elution time, obtained using the calculated and measured hydrodynamic diameter (D_h) vs peak apex elution time for polystrene polymers (PS stds) and linear hydrocarbons (C_k stds) for (a) single-column pore size 100 Å (PL100) and 1000 Å (PL1000) and (b) single-column, high-resolution 1000-Å pore-size column (HR3) compared to two such columns used in series (HR3 + HR3).

We typically add other surfactants such as amines or thiols after the reduction is complete (this occurs in less than 30 s for strong reducing agents such as $LiAlH_4$!). Nonetheless, to ensure that the reductant is completely exhausted, we wait about an hour after the reduction before adding the passivating agent. For surfactants that bind somewhat weakly to the nanocluster surface, such as nonionic surfactants in the polyether family C*i*E*j*, slow growth of the clusters occurs after complete reduction, so the amount of time one waits before adding a strongly binding passivating agent can be used to obtain a desired average nanocluster size (see, for example, Au 487 b, c, d; Table 1, 2). We will discuss the effect of age on the nanocluster average size and size distribution further below.

We also studied systems such as those described by Whetten et al.,[12] in which the thiol is added prereduction and thus competes with the surfactant for the complexation of the precursor gold salt (see Au 508, 536−538, 565p−567p). As we shall see, the general effect of such competition is to reduce the final nanocluster size for a fixed Au salt concentration, reducing agent, and surfactant system as well as producing a narrower size distribution. We find that there is very little further effect on the final cluster size or size distribution once the thiol concentration is equal to or greater than the Au concentration (compare Au508, 537, 538; Table 2).

Size Dependence of the Elution Time. SEC has long been the method of choice for determining the size distribution of polymers, but how can one utilize SEC to study these properties in a system of metal nanoclusters? To show first how molecules elute from an SEC column, we show in Figure 1a the peak elution time versus the measured and/or calculated hydrodynamic diameter for nearly monodisperse polystyrene (PS) size standards (Polymer Labs) and ordinary monodisperse alkyl hydrocarbons. In the case of the PS standards, we can calculate their hydrodynamic diameter from parameters available in the *Polymer Handbook* and directly measure their hydrodynamic diameter by DLS. For the larger (e.g., >3000 MW) PS standards, we both calculated and

(14) Yau, W. W.; Kirkland, J. J.; Bly, D. D. *Modern Size-Exclusion Liquid Chromatography*; Wiley-Interscience: New York, 1979.
(15) Fischer, Ch. H.; Lillie, J.; Weller, H.; Katsikas, L.; Henglein, A. *Ber. Bunsen-Ges. Phys. Chem.* **1989**, *93*, 61.
(16) Fischer, Ch. H.; Weller, H.; Katsikas, L.; Henglein, A. *Langmuir* **1989**, *5*, 429.

measured their hydrodynamic diameter, and the agreement was excellent. Similar size information is available in the literature for linear hydrocarbons in toluene. The resulting semilog plot of Figure 1a convincingly demonstrates that for a pure SEC separation mechanism, $\log D_h \sim t_r$, where t_r is the elution (or retention) time (apex of the elution peak), as measured with one of our HPLC detectors (refractive index detector in this case), and D_h is the hydrodynamic diameter of the analyte in the mobile phase (toluene in this case). Note that both the hydrocarbon standards, hexane through hexadecane, and the PS standards fall on the same curve, showing that only the average hydrodynamic diameter is important.

This figure shows that the same behavior is observed on both the PL1000 and PL100 SEC columns (1000- and 100-Å pores, respectively). However, the column with larger pores can separate larger polymers than the one with smaller pores, but it does not have as good a resolution (2 Å vs 4 Å). The upper limit of size fractionation is called the total exclusion limit, and as its name suggests, any molecule bigger than this size will be totally excluded from the pore volume, with no size discrimination occurring. At long elution times, all the molecules are so small that they penetrate all the pore volume and elute at essentially identical times. Only in the time region between these limits does size discrimination occur. Finally, if a molecule has an affinity for the column (e.g., polar molecules such as THF, acetonitrile (ACN), or methanol (MeOH)), this further retards their progress through the pores, and a pure SEC separation mechanism no longer occurs. This must be avoided if we want to obtain nanocluster size information from SEC.

There are various tests we can apply to see if a passivated nanocluster has a binding affinity with the column. A strong indication is an asymmetrical elution peak with a lot of "tailing" on the longer elution time tail. (This is almost always observed with surfactants, molecules with a strong affinity for surfaces.) Another way to detect specific chemical interactions is to study the dependence of the elution time on the amount of material injected onto the column. The elution time should be independent of the amount of material injected over a wide range of injection amounts. A third test is to remove the column completely, measure the total number of clusters that elute by using the absorbance chromatogram elution area at a particular wavelength, and then compare this to the same absorbance elution peak area with the column. For the best samples, between 90 and 100% of the clusters elute. All the samples in Table 2 satisfy these three criteria. We make these tests to ensure that we can interpret the elution time in terms of the hydrodynamic diameter of the capped nanocluster.

The pore size of the column must be within the range appropriate for the capped nanoclusters. For example, one can see from Figure 1a that if a nanocluster sample has a size between 0.5 and 4 nm that a PL100 column would give the best separation, whereas for clusters with sizes up to 10 nm the PL1000 would be more useful. However, with SEC one can literally have it all, as shown in Figure 1b. Here, we show calibration curves on high-resolution (HR3) 1000-Å pore columns made by Waters Corp. using the same standards described in the previous paragraph. We show both a single column and two columns attached serially. Note that the effect of the additional column is to spread out the separation between similarly sized polymers (i.e., the slope of $\log D_h$ vs t decreases because the available pore volume doubles), whereas the inherent line width (defined by the elution time width of a monodisperse species such as octane) remains almost

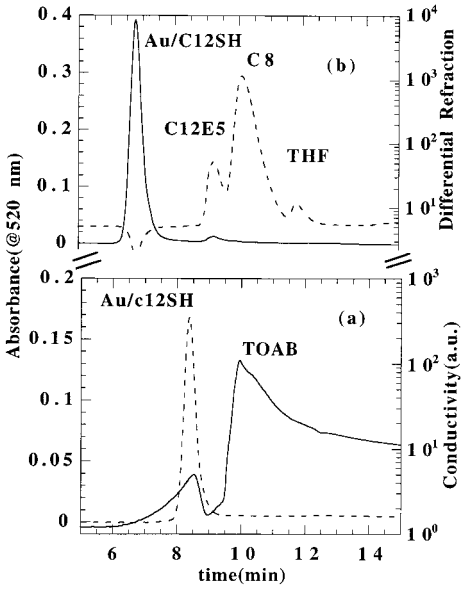

Figure 2. Chromatographic separation of capped Au nanoclusters. (a) Sample #470b, obtained using a PL500 column and a toluene mobile phase. A coplot of the absorbance at 520 nm, A(520 nm), and the differential refraction vs elution time shows the separation and detection of Au nanoclusters and the other chemicals used in their preparation—a nonionic surfactant (C12E5), the solvent (C8 = octane), and THF (to dissolve the reducing agent, $LiAlH_4$). (b) Au #538 nanoclusters are separated from a cationic surfactant, TOAB. Coplot of A(520 nm) and the conductivity vs elution time.

constant. So, simply by adding more pore volume, we obtain 1−2-Å size discrimination compared to 2−4 Å with a single column. The only price to pay for this increase in size discrimination is that the sample takes about twice the time to elute from the column. However, this poses no penalty if one increases the flow rate of the mobile phase. This strategy of increasing the pore volume to increase the resolution can be taken to the extreme of using a preparative SEC column with roughly 10× the volume of the columns shown in Figure. 1. Such columns are used by pharmaceutical companies to fractionate biopolymer samples differing by less than 2% in hydrodynamic size, and since they have so much pore volume, they can be used with enormous volumes (1−2 mL) of injected samples, allowing hundreds of milligrams of purified, size-fractionated molecules to be prepared in a few hours.

From the above discussion, we can use HPLC to study both the synthesis and purification of gold nanoclusters, as well as to investigate their size distributions and optical properties. The optical properties will be presented in more detail in a paper in preparation. We first show results concerning purification.

Nanocluster Purification. Gold nanoclusters, after synthesis in inverse micelles, contain byproducts. These impurities can be observed by HPLC using multiple detectors such as a PDA for absorbance and an RI detector to monitor the nonabsorbing organic surfactants, as shown in Figure 2a. Since the RI detector sensitivity is low for cationic surfactants in toluene, we use a conductivity detector and THF as the mobile phase to monitor for ionic species (Figure 2b).

Liquid-Phase Extraction. We use liquid-phase extraction to remove the impurities from samples prepared in alkanes. Because these solvents are immiscible with polar organic solvents like formamide (FA), *N*-methyl formamide (NMF), and methanol, we have found that NMF, with its extraordinarily high dielectric constant, is effective in

extracting all the ions and surfactant from thiol-stabilized nanoclusters.

Liquid−liquid extraction, commonly used to purify ordinary chemicals, is quite general for a wide range of surfactants and metal nanoclusters, although the partitioning ratio is dependent on the degree of hydrophilicity of the surfactant (e.g., the *i*/*j* ratio determines how hydrophobic the nonionic surfactant C*i*E*j* is, so decreasing this ratio leads to more extraction into the immiscible polar organic phase).

Solid-Phase Extraction. Solid-phase extraction of byproducts from a nanocluster solution is based on the differences in either size or chemical affinity of Au nanoclusters compared to chemical impurities. For small quantities of nanoclusters, for example, 1−100 mg, we employed a custom-designed HPLC fraction collection system to isolate different sized clusters and to remove other chemicals from monodisperse clusters. This system employs a computer-controlled microvalve switching system that directs the mobile phase at a given point in the elution time through a small Teflon tube and stainless steel needle that penetrate a septum-sealed vial. This system can have collection vessels of arbitrary volume and can be completely air-free, and the collection can be triggered either by the PDA signal exceeding a predetermined absorbance level at a particular wavelength or on a time basis, relative to the start signal at the injection time and using the known elution time of the desired nanoclusters. In the case of polydisperse samples, one can visually observe the size-dependent color of the different fractions of the elution peak collected. This is particularly true of bimodal size distributions with two baseline-resolved peaks. For example, the fastest eluting fractions (largest nanoclusters) are red, whereas late eluting fractions are orange.

For faster purification of larger amounts of a sample, solid-phase extraction cartridges are available (e.g., Water's Corp. Sep-Pak) that contain the same types of materials used in HPLC columns. These disposable cartridges of organically functionalized silica, alumina, or ion exchangers are able to retain polar or ionic materials while passing nonpolar ones such as alkane thiol-stabilized Au nanoclusters. They are commonly used to concentrate analytes prior to chemical analysis, but they work well for purifying nanoclusters. We found the hydrophilic columns of silica and alumina to be the most useful for purification, as the hydrophobic nanoclusters pass freely through these materials while ions and surfactants are retained. The final nanocluster solution purity after two to three passages through the cartridge is quite good, as monitored by HPLC analysis of the clusters.

Precipitation. Precipitation of nanoclusters from solution by adding a nonsolvent has been employed by many researchers.[17] Unlike liquid extraction, it is more difficult to use with nanoclusters prepared in alkanes, since the polar, organic nonsolvents such as methanol, ethanol, or NMF typically used to precipitate the alkane thiol-stabilized nanoclusters from solution are immiscible in alkanes. We have discovered that cold acetone or 2-propanol does permit nanocluster precipitation from alkane solutions in many cases, but nanocluster recovery is lower (∼20−50%) compared to liquid-phase extraction (80−100%). However, precipitation is effective for removing surfactants from toluene-based inverse micelle solutions while recovering nearly 100% of the as-synthesized gold nanoclusters.

(17) Schaaff, T. G.; Shafigullin, M. N.; Khoury, J. T.; Vezmar, I.; Whetten, R. L.; Cullen, W. G.; First, P. N. *J. Phys. Chem. B* **1997**, *101*, 7885.

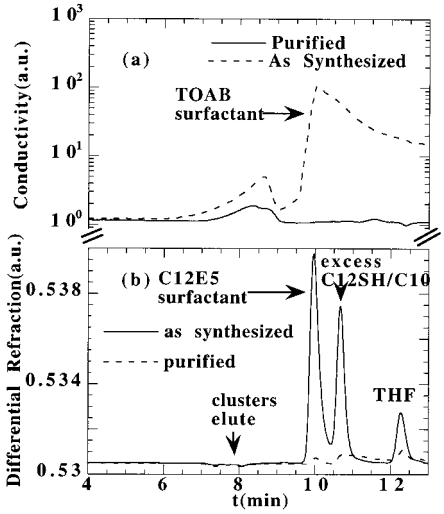

Figure 3. Purification of Au nanoclusters. (a) Au #538 nanoclusters purified by MeOH precipitation. Conductivity vs elution time for as-synthesized and purified Au nanoclusters. (b) Au #463a purified by NMF extraction. The differential refraction vs elution time for as-synthesized and purified Au nanoclusters is shown.

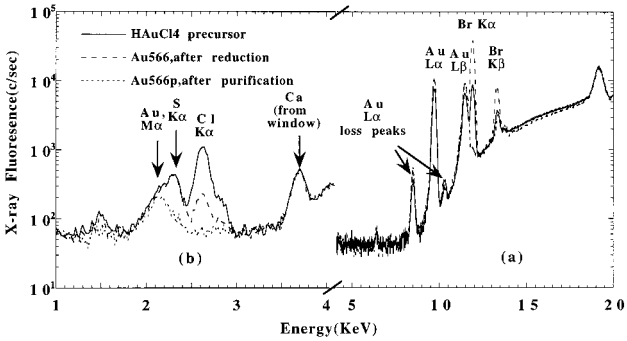

Figure 4. (a) XRF analysis of Au and Br concentrations before and after purification of Au #566. (b) XRF analysis of Au, S, and Cl concentrations before and after purification of Au #566.

Figure 3a shows the HPLC conductivity signal before and after methanol precipitation for Au538 (see Tables 1 and 2) nanoclusters in toluene. We use a 10-fold excess MeOH volume, allow the nanoclusters to precipitate for ∼1 h, and then centrifuge at 100 g for 15−30 min. This chromatogram reveals that the *unpurified* Au nanoclusters do have some conductivity, presumably due to adsorbed cationic surfactant, so the thiol does not displace all the cationic surfactant when it is added. However, purification renders the nanocluster basically neutral.

Figure 3b shows the RI signal before and after purification of the sample Au463a, prepared using the nonionic surfactant C12E5 in toluene and extracted twice using NMF. The surfactant, chemicals used in reduction, and excess thiol are nearly completely removed. The elution of the Au nanoclusters cannot be detected by the RI detector.

To determine the extent of surfactant and thiol removal via precipitation and to monitor the inorganic elements directly, we performed X-ray fluorescence (XRF) analysis (Spectrace QuantX system). Figure 4a shows the XRF analysis of Au566, from the precursor to the final purified sample. Little or no change in Au concentration was observed, while the Br concentration went from an initial value of 0.06 M to 0.031 M after reduction and placing the sample in contact with water, to 0.0002 M after MeOH precipitation. The characteristic Br Kα peak completely disappears, as this figure shows. In Figure 4b, obtained

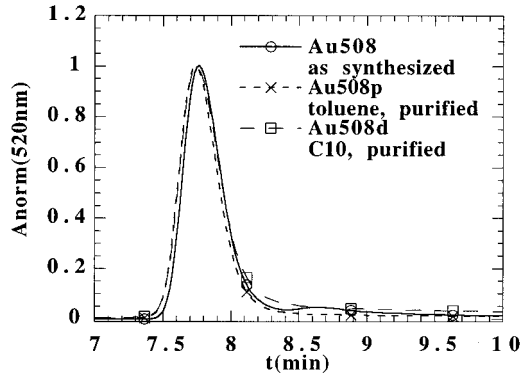

Figure 5. Nanocluster size distribution is unaffected by the purification method. Chromatogram showing the peak-normalized absorbance vs elution time for Au, in which the clusters were precipitated (#508p), and the surfactant was precipitated, (#508d), compared to the as synthesized parent (#508).

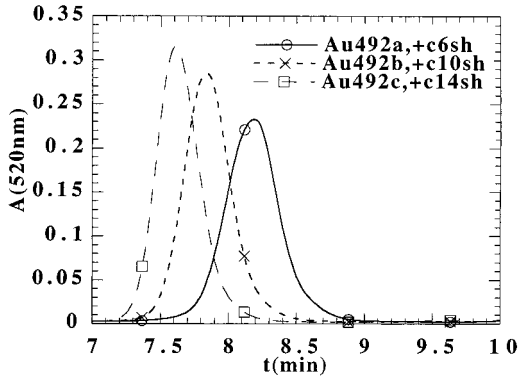

Figure 6. Effect of capping agents on the hydrodynamic diameter of Au #492 nanoclusters. HPLC chromatogram of Au nanoclusters with three alkanethiols, C*k*SH, $k = 6$, 10, and 14, added after reduction. The absorbance at 520 nm $A(520\text{ nm})$ from the PDA vs elution time is shown. The SEC column used was a Polymer Labs PL1000, and the mobile phase was toluene at a 1 mL/min flow rate.

under different X-ray fluorescence excitation conditions and using a He purge to increase S/N, we monitored the Cl concentration (from the precursor $HAuCl_4$ salt) and the S concentration (from the 0.03 M C12SH addition) signals. Since the Au Mα and S Kα lines overlap, we calculated the remaining S peak from the total area, subtracting off the Au Mα line area from the known Au concentration. The sulfur concentration decreased from 0.03 M to 0.001 M, and the initial Cl concentration of 0.04 M decreased to zero (our Cl detection limit is 30 ppm for our instrument) after purification. For these $d \sim 2$ nm clusters, this concentration of S yields a Au:S ratio of 10:1. This is the typical [Au]:[S] ratio we have observed in this size range, independent of alkyl chain length for $8 < k < 16$.

We purified several samples containing various chain-length alkanethiols a second time by MeOH precipitation but discovered, as have others,[18] that excess purification washes the alkanethiols off the clusters, leading to instability and even plating out of the clusters. It is also often found that the Au clusters will not precipitate a second time without aggressive centrifugation, which compacts the nanocluster pellet to such an extent as to render redissolution almost impossible.

Several researchers assert that precipitation of nanoclusters from solvent/nonsolvent pairs is "size selective", in contrast to our experience—that it merely discriminates based on the surface chemistry of the hydrophobic Au nanoclusters.[12,13] If size discrimination is really occurring, then HPLC before and after precipitation should show a change in the cluster elution time (size) and/or peak width (size distribution). Figure 5 shows, for Au508, that both the as-synthesized and the precipitated nanoclusters (Au508p) have identical elution times (sizes) and line widths (size distribution). We also purified the parent sample Au508 by evaporating off the toluene, then redissolving the C12SH-stabilized nanoclusters in decane, a solvent in which TOAB has negligible solubility (sample Au 508d). This method of purification also left the average size and size dispersion invariant. This is expected since all the nanoclusters are recovered by this method: only the surfactant and ionic impurities are removed. We have never observed any size discrimination by precipitation in the samples we prepared by the inverse micelle process and purified by precipitation. Instead, we have sometimes observed, with special surfactant/reducing agent combinations, subpopulations of nonprecipitating clusters whose surface properties are essentially hydrophilic and thus, they fail to bind the alkanethiols strongly enough to compete with the cationic surfactant, which is usually quite soluble in MeOH. HPLC has shown that such clusters do not differ in size from the hydrophobic clusters.

Size Distributions from HPLC. To use SEC to obtain absolute cluster sizes, one needs nanocluster "standards" to develop a calibration curve. To develop standards, we prepare monodisperse solutions of nanoclusters with a single Au core size and then stabilized these clusters using 3 different alkanethiols of known chain length. Using HRTEM, one then obtains the core size of each sample and, assuming the shell thickness added by the thiols is independent of core size, one can obtain the total (core + shell) diameter by assuming the calibration curve(s) of Figure 1 to be valid. By subtraction, one can then obtain the shell thickness due to the alkyl capping group. Further verification of this procedure was obtained by running the samples on another pore size column and comparing the D_h values obtained using its calibration curve.

Figure 6 shows that for a single core size (Au492a,b, and c, 2.0-nm core by HRTEM), the elution time varies as predicted with alkyl chain length. The nanoclusters with the smallest shell thickness elute at the longest time. Now, using the PS-based calibration curve for this PL1000 column (Figure 1a, whose best fit is $D_h(t) = 608\exp(-0.62525t)$), one obtains the hydrodynamic (core + shell) diameters shown in Table 2. After subtraction of the known HRTEM core size of $2.0 \pm (0.2)$ nm, one obtains the total shell thicknesses indicated, 13.9 (C6SH), 21.9 (C10SH), and 28.7 Å (C14SH), respectively. Using the PL500 column, one obtains 14.2, 21.0, and 26.6 Å for the same samples. These values should be twice the alkyl chain length in solution, and they appear to be consistent with this assumption, which predicts about an 8-Å shell thickness increase for every 4 carbon atoms added to the alkanethiol passivating agent; this implies a 1.0-Å linear C−C distance in toluene solution, very close to what we find from our calibration curve of free hydrocarbons shown in Figure 1. The assumption of an alkanethiol shell thickness that does not depend strongly on core diameter may not hold well for significantly larger core sizes. We do know, for example, that alkanethiols do not adsorb as strongly on larger, $d > 5$ nm Au, clusters, suggesting that the thickness of the passivating layer might decrease.

To check the consistency of our analysis, we then synthesized other samples, also monodisperse as verified by SEC and HRTEM and obtained the elution times and

(18) Korgel, B. A.; Fullam, S.; Connolly, S.; Fitzmaurice, D. *J. Phys. Chem. B* **1998**, *102*, 6319.

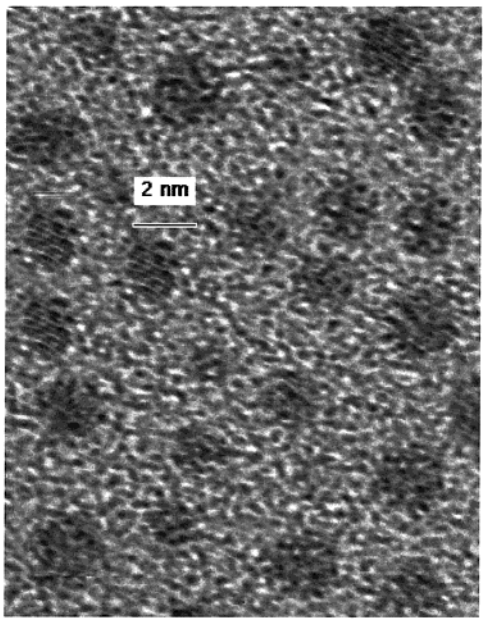

Figure 7. HRTEM of a region of a holey carbon grid on which a drop of sample Au508p was allowed to dry.

total hydrodynamic diameters shown in Table 2. Using the shell thicknesses obtained above, we can calculate the core size from the hydrodynamic diameter obtained from the calibration curve of Figure 1. These core sizes are in good agreement with TEM sizes. The largest uncertainty in this analysis is the HRTEM measurements of core size for the small nanoclusters. As an example, we show an HRTEM in Figure 7 of Au508p ,whose size from Table 2 is given as 2.0 ± 0.2 nm. Although Figure 7 is consistent with this size, there is no objective method of determining whether the true size distribution is as narrow as indicated from HPLC, due to the effects of grid/particle contrast and particle orientation and whether the particle lies in the focal plane.

HPLC Line Width. Even for perfectly monodisperse samples such as toluene, an HPLC system has instrumental (column and detector) line width. For example, the full width at half-height (fwhh) of decane run in a mobile phase of toluene on a PL1000 column at 1 mL/min is 0.3 min. For our polymer-size standards, the fwhh is 0.5 to 0.6 min even though our PS standards are exceedingly monodisperse, with M_w/M_n (M_w = weight-average molecular weight, M_n = number-average molecular weight) values as low as 1.05. So a high resolution SEC column can detect fairly minute variations from monodispersity.

Comparing the line width of solid, roughly spherical objects such as gold nanoclusters to polymer coils might affect our estimates of the cluster size distribution. Fortunately, there are "solid" molecules with dimensions roughly comparable to our nanoclusters, namely C60 and C70. The latter is available in highly purified (by HPLC!) form from Strem Chemicals (99.9%), and both C60 and C70 are soluble in toluene.

Figure 8 shows the normalized elution peaks of C60 and Au 470b run under identical conditions on a PL500 column with toluene as the mobile phase. The elution time of C60 is shifted to match that of the Au nanoclusters. The line width of the nanoclusters is actually slightly narrower than C60. Its fwhh is 0.4 min, as compared to 0.3 min for a molecule such as C10 run on this same column, so it appears that neither sample is perfectly monodisperse. The slight asymmetry in the elution profile

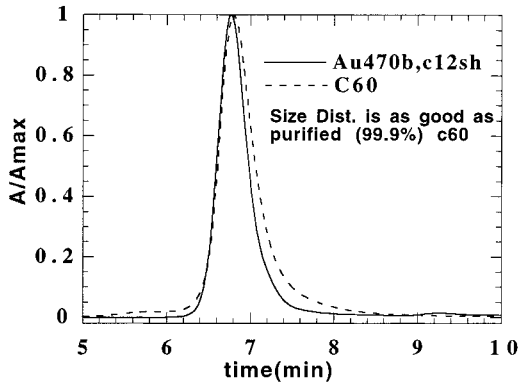

Figure 8. Size distribution of Au clusters is as narrow as buckyballs. Normalized absorbance chromatogram from a PDA detector (A/A_{max}) for C12SH-stabilized Au nanoclusters and 99.9% C60. HPLC conditions were a PL500 column with toluene as the mobile phase, flowing at 1 mL/min. The C60 elution time was shifted to coincide with that of the Au nanoclusters for ease of comparison.

of C60 might be due to a surprising tendency of C60 to interact with the column but could also be an indication of some size dispersity in the 99.9% sample. In any case, the narrow size distribution of our best Au nanocluster samples is evident.

We assume that the inherent instrumental line width σ_I of our best nanocluster sample is the same as that observed with nearly monodisperse Au samples such as Au470b or 508p. Then, since the convolution of two Gaussian peaks is a Gaussian, the total line width σ_T of a sample due to polydispersity, σ_D and instrumental effects is given by

$$\sigma_T^2 = \sigma_d^2 + \sigma_I^2 \quad (1)$$

Equation 1 allows us to compute the sample polydispersity, using the measured instrumental width of 0.3 min for a PL1000 column and the sample line width. From σ_D, one can then use Figure 1, the calibration curve for this column, to estimate the spread in cluster sizes. To use HPLC to analyze for average size and size dispersion, at least two additional variables, nanocluster shape and specific interactions with the column, must be considered, however.

Nanocluster shape can play a role in the observed elution time. This is nicely illustrated by comparing the elution of a roughly spherical cluster like C60 to that of a more football-shaped, but larger, C70 cluster. If overall molecular weight were the only consideration, we would expect the larger C70 cluster to elute more quickly than C60, but just the opposite is observed in Figure 9. In fact, both C60 and C70 elute at much later times than decane, C10, which is hydrodynamically smaller, indicating that both molecules interact (i.e., stick) with the polystyrene gel column. Even though their elution times do not permit us to obtain their absolute size, they are easily separated by their different shapes (it is unlikely that they have different chemical affinities for the column material since they are both made of carbon). In our analysis of Au cluster sizes, we will assume that the clusters are spherical.

As mentioned previously, an indicator of specific chemical interactions of a cluster with the column is the asymmetry of the elution peak. Any chemical interaction with the column will slow the nanocluster elution compared to a pure SEC mechanism, leading to an *underestimate* of the cluster size. The self-consistency of the observed hydrodynamic volume for several different

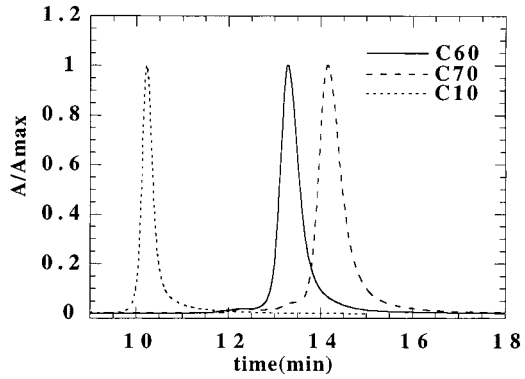

Figure 9. Chromatogram instrumental line width for samples of decane (C10), C60, and C70 run on a PL500 column in toluene.

columns, as illustrated in Table 2, helps to rule this out, as well as indicating the reproducibility of cluster size measurements. The astute reader will note a small but significant difference in the observed shell thickness for the PL500 and PL1000 columns in the case of larger, $d > 5$ nm, clusters.

In Table 2, we have converted the HPLC line width into a size distribution by using the best fit to the data of Figure 1. These values are shown in this table only for the case of the best (narrowest inherent instrumental line width) PL1000 column, since the elution peaks were not as symmetrical for the same samples on the HR3 and Pl500 columns. Also worth noting is the larger polydispersity for a given sample chromatographed using two PL1000 columns (pl1000 × 2), which give superior size resolution. These chromatograms were obtained when the samples were considerably (6 months ∼ 1 year) older, when we decided to increase the column total volume, and so the increased dispersity might reflect an aging effect. Obviously, the uncertainties in determining polydispersity are greatest for nanoclusters with line widths close to the instrumental value. Still, these are probably the most objective values currently available for size dispersity in Au nanoclusters.

Conclusions

HPLC is a powerful size analysis, separation, and characterization tool well suited to the examination of metal and semiconductor nanoclusters in the size regime where strong quantum confinement effects are important. In this regime the largest single uncertainty in nanocluster measurements is often the ability to determine absolute size and size dispersion in a sample for comparison to observed physical properties such as optical absorbance, PL, and so forth. We have shown how absolute sizes and size dispersions can be rapidly obtained by SEC chromatography. In particular, we demonstrated that Au nanoclusters passivated with alkanethiol shells follow ideal SEC behavior, namely, $\log D_h \sim t_r$, where t_r is the retention time and D_h the hydrodynamic diameter. We were also able to measure the organic shell thickness for the first time, for $k = 6-18$.

We observed that in the size regime below $d \sim 3$ nm, certain retention times and sizes are observed quite independently of widely differing synthetic variations. We attributed these observations to especially stable "magic" sizes. By analysis of the elution peak line widths, we also showed that such samples are remarkably monodisperse, exceeding that of purified C60 standards, and furthermore that these elution times and line widths are stable for periods of over a year.

A significant aspect of the ability to use SEC for size determination is the ability to passivate the inorganic nanocluster surface to allow the nanocluster to flow through the porous organic media of the SEC column without having specific interactions with the column, which would give spurious elution times and hence, sizes. This was accomplished by learning how various organic passivating surfactants bind to metal cluster surfaces using HPLC.

In a previous paper,[19] we showed how HPLC combined with an on-line fluorescence detector can be used to discover novel, size-dependent PL properties of Au nanoclusters while convincingly removing any impurities that might give spurious PL signals. Although space considerations preclude a detailed discussion, the use of this size information combined with the complete absorbance data from our PDA allows a detailed examination of the cluster size dependence of the optical plasmon absorbance of both Au and Ag nanoclusters. We will present these results in another paper. In the future, we feel HPLC will significantly augment and enhance present size determination methods such as TEM and will add to our knowledge of the size-dependent properties of nanoclusters.

Acknowledgment. This work was supported by the Division of Materials Sciences, Office of Basic Energy Sciences, of the U.S. Department of Energy under Contract DE-AC04-94AL8500. Sandia is a multiprogram laboratory operated by Sandia Corporation, a Lockheed-Martin Company, for the U.S. Department of Energy.

LA000669J

(19) Wilcoxon, J. P.; Martin, J. E.; Parsapour, F.; Wiedenman, B.; Kelley, D. F. *J. Chem. Phys.* **1998**, *108*, 9137.